Journal of Medicinal Chemistry

Brief Article

Co-Localization Strategy Unveils an Underside Binding Site in the Transmembrane Domain of Smoothened Receptor

Fang Zhou, Kang Ding, Yiqing Zhou, Yang Liu, Xiaoyan Liu, Fei Zhao, Yiran Wu, Xianjun Zhang, Qiwen Tan, Raymond C. Stevens, Fei Xu, Wenfu Tan, Youli Xiao, Suwen Zhao, and Houchao Tao

J. Med. Chem., **Just Accepted Manuscript** • DOI: 10.1021/acs.jmedchem.9b00283 • Publication Date (Web): 13 Aug 2019

Template for Submission of Manuscripts to American Chemical Society Journals

Word 2010, Page Wide Abstract Version

This template is a guide to be used to prepare manuscripts for submission. Please consult the Instructions to Authors or a recent issue of the journal for detailed guidelines and procedures for submission. This template is intended to benefit to the author in that the entire manuscript (text, tables, and graphics) may be submitted in one file. Inserting graphics and tables close to the point at which they are discussed in the text of the manuscript can also be a benefit for the reviewer.

When you submit a manuscript using this template, you will not actually see the page formatting that appears in the printed journal. This will occur as part of the editorial production process. Abbreviated instructions for using the template follow. Consult the documentation for your specific application and version for more information. Additional instructions can be found in the readme file at the web page where you downloaded this template.

Using the template

In ACS publications there are many different components of a manuscript (i.e., title, abstract, main text, figure captions, etc.) that are represented in the template. See the Guide, Notes, Notice, or Instructions for Authors on the journal's homepage to determine which parts should be included for the manuscript that you are preparing

1. If typing your manuscript directly into the template, select (highlight) the text of the template that you want to replace and begin typing your manuscript (i.e., select the Title section for typing in your title).
2. If you have already prepared your document in a Word file, you will need to attach the template to your working document in order to apply the Word Style tags. Further instructions can be found in the readme file at the web page where you downloaded this template.
    a. Go to the Word Style list on the formatting toolbar and you will see all the Word Styles from the template that has now been imported into the current document. A Styles toolbar has been generated that will display the different Styles for you to choose from. If this is not present, select **View**, **Toolbars**, and then select **Styles** and it should appear. You can close this at any time and then reopen it when needed.
    b. Click in the sentence or paragraph and then go to the Word Style menu on the toolbar and select the relevant Word Style. This will apply the Word Style to the entire text (sentence or paragraph). Do this for all sections of the manuscript.
3. To insert graphics within the text or as a figure, chart, scheme, or table, create a new line and insert the graphic where desired. If your graphic is not visible, ensure that the Word Style is "Normal" with an automatic height adjustment. If the size of the artwork needs to be adjusted, re-size the artwork in your graphics program and re-paste the artwork into the template (maximum width for single-column artwork, 3.3 in. (8.5 cm); maximum width for double-column artwork, 7 in. (17.8 cm)). **NOTE**: If you are submitting a Table of Contents graphic, please insert the graphic at the end of the file.
4. Ensure that page numbers are present on all pages before submitting your manuscript.
5. Delete these instructions and any sections that are not needed.
6. Save the file with the graphics in place: select **Save As** (**File** menu) and save it as a document file (not a .dot template file).
7. Proof the manuscript to ensure that all parts of the manuscript are present and clearly legible.

Co-Localization Strategy Unveils an Underside Binding Site in the Transmembrane Domain of Smoothened Receptor

Fang Zhou[1,2,5,6†], Kang Ding[1,3,5,6†], Yiqing Zhou[4†], Yang Liu[1], Xiaoyan Liu[1], Fei Zhao[1], Yiran Wu[1], Xianjun Zhang[1,5,6,8], Qiwen Tan[1], Raymond C. Stevens[1,6], Fei Xu[1,6], Wenfu Tan[7], Youli Xiao[4,5*], Suwen Zhao[1,6*], and Houchao Tao[1*]

[1]iHuman Institute, ShanghaiTech University, Ren Building, 393 Middle Huaxia Road, Pudong New District, Shanghai 201210, China

[2]Shanghai Institute of Materia Medica, Chinese Academy of Sciences, 555 Zuchongzhi Road, Building 3, Room 426, Shanghai 201203, China

[3]Key Laboratory of Computational Biology, CAS-MPG Partner Institute for Computational Biology, Shanghai Institutes for Biological Sciences, Chinese Academy of Sciences, Shanghai 200031, China

[4]CAS Key Laboratory of Synthetic Biology, Institute of Plant Physiology and Ecology, Shanghai Institutes for Biological Sciences, Chinese Academy of Sciences, Shanghai 200032, China

[5]University of Chinese Academy of Sciences, No. 19A, Yuquan Road, Beijing 100049, China

[6]School of Life Science and Technology, ShanghaiTech University, Shanghai 201210, China

[7]Department of Pharmacology, School of Pharmacy, Fudan University, Shanghai 201203, China

[8]Institute of Biochemistry and Cell Biology, Shanghai Institutes for Biological Sciences, Chinese Academy of Sciences, Shanghai 200031, China.

Supporting information

ABSTRACT: We unveiled an underside binding site on smoothened receptor (SMO) by a co-localization strategy using two structurally-complementary photoaffinity probes, derived from a known ligand Allo-1. Docking study and structural dissection identified key interactions within the site, including hydrogen bonding, π-π interactions, and hydrophobic interactions between Allo-1 and its contacting residues. Taken together, our results reveal the molecular base of Allo-1 binding and provide a basis for the design of new-generation ligands to overcome drug resistance.

INTRODUCTION

Hedgehog (Hh) signal transduction is of vital importance in the regulation of embryonic development and adult tissue maintenance[1-2]. This pathway is initiated by the binding of the Hh protein to the receptor Patched1 (Ptch1), which releases the inhibition of Ptch1 to the smoothened receptor (SMO) and eventually induces the expression of target genes[3]. However, over-activation of the Hh pathway is associated with the initiation of several human tumors, suggesting SMO as a target of anti-tumor therapeutic development[4-6]. Pharmaceutical efforts have resulted in several FDA-approved drugs, including vismodegib and sonidegib for the treatment of basal cell carcinoma, the most common skin malignancy[7], and glasdegib for treatment of acute myeloid leukemia, the most common type of acute leukemia in adults[8]. However, drug-resistant mutation of SMO often occurs after clinical use of these drugs[9]. For example, the D473H mutant, identified from tumor relapse, showed significant attenuated binding to vismodegib[10-12]. Thus far, exploring novel small-molecule ligands with alternative mechanisms to overcome drug resistance caused by SMO mutation remains challenging[13].

The tremendous progress in structural biology has resulted in a plethora of SMO research[14]. To date, several high-resolution structures of human SMOs have been resolved, including 7-transmebrane domain (TMD) and extracellular domain (ECD), as well as multi-domain SMO reported recently [15]. Most of these SMO structures are bound to small molecule ligands, including the antagonists (cyclopamine (CP), SANT-1, LY0940280) and agonists (SAG) in traditional TMD, and sterols in ECD (Figure S1)[16-21].

In the past decades, thousands of allosteric modulators targeting GPCRs have been developed. However, a limited number of binding poses (less than 20) have been elucidated due to low binding affinity and incomplete structure-activity relationship (SAR) information. Structural studies have contributed substantially to understanding of the SMO function[22], but the binding sites of several significant allosteric ligands remain unknown (Figure S2). Allo-1 is one of the most well-known allosteric ligands that maintain inhibitory activity against drug-resistant mutant SMO, but few analyses of SAR have been carried out [10, 15]. According to previous studies, Allo-1 binds to neither TMD nor ECD, where multiple known ligands bind (Table S1)[23,17, 19, 24-25]. Confusingly, the effective competition of Allo-1 with BODIPY-CP (Figure S3), a classic fluorescent probe derived from CP, indicated that Allo-1's binding site probably overlaps the occupancy of the

BODIPY moiety but not of CP. However, this finding was not supported by our docking and simulation studies (Figure S4). The undergoing program of co-crystallization has not been successful yet to unmask cryptic binding. As part of our continuous efforts in structural studies and therapeutic development on SMO, we report the determination of an underside binding site for Allo-1 by using an integrated approach combining photoaffinity labeling, computational modeling and structural dissection study.

RESULTS AND DISCUSSION

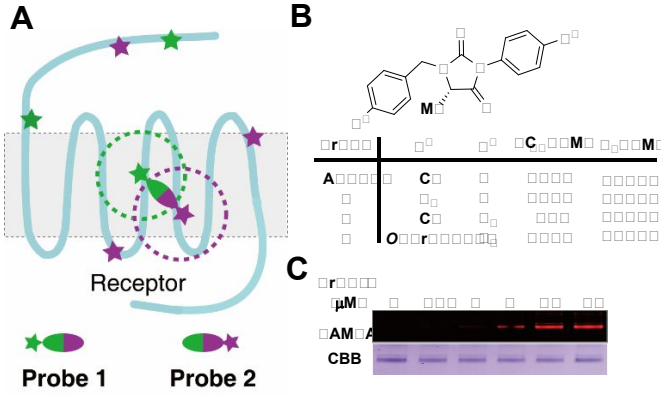

Figure 1. Design and characterization of the photoaffinity probes (**1**-**2**). (A) Definition of a new ligand binding site by using co-localization strategy by connecting two modified areas caused by two probes. (B) Structures of Allo-1 and derived probes with azido groups at the two ends. The potency of the analogs was evaluated by the Gli-luciferase reporter assay, and binding affinity was evaluated by fluorescence-based competition test with Bodipy-LY. IC_{50} and K_i values represent the mean ± SEM of three independent experiments, each at least in duplicate. (C) SDS-PAGE analysis and fluorescence detection indicated the specific conjugation of probes with the SMO. Dually purposed probe **3** incubated with SMO protein was irradiated with UV light for 30 min, followed by "click" conjugation to tetramethylrhodamine-azide (TAMRA-N_3).

Design and characterization of Allo-1-derived photoaffinity probes. To elucidate Allo-1 binding, we developed photoaffinity ligands[26-27]. Upon irradiation with UV light, active intermediates, such as nitrene or carbene, trap the target proteins through covalent alkylating of adjacent amino acid residues, which could be interpreted by proteolysis and mass spectroscopy[28]. Ideally, the binding region of the ligand could be navigated around the spherical area centered by the alkylated residues, which often involve a time-consuming trial and error procedure. Inevitably, nonspecific labeling often occurs, thereby complicating the identification. Herein, we introduced a co-localization strategy (Figure 1A) that rapidly and accurately defines the binding area by simply connecting the two modified areas caused by two probes. Only the connection that matches the size of the ligand can be a potential site for further docking study. To this end, two probes **1** and **2** were designed by installing azido groups at both ends of Allo-1, i.e., at the para-substituent of either benzene moiety (Figure 1B and Scheme S1)[29]. Both probes, together with bifunctional probe **3** bearing one more terminal alkyne tag, exhibited comparable antagonism in the luciferase reporter assay and binding affinity in the fluorescence-based competition test compared with the parent compound Allo-1; this finding indicates that the introduction of a small linear azide and a propagyl group was largely tolerated (Figure 1B). The specificity of the probe was further demonstrated in a two-step treatment of probe **3** (Figure 1C) and competition test in the presence of Allo-1 (Figure S5). In comparison, another photoactivable group diazirine was not allowed because its introduction to Allo-1 (probe **4**, Figure S6) led to a significant loss of activity, due to size incompatibility[29, 30-31].

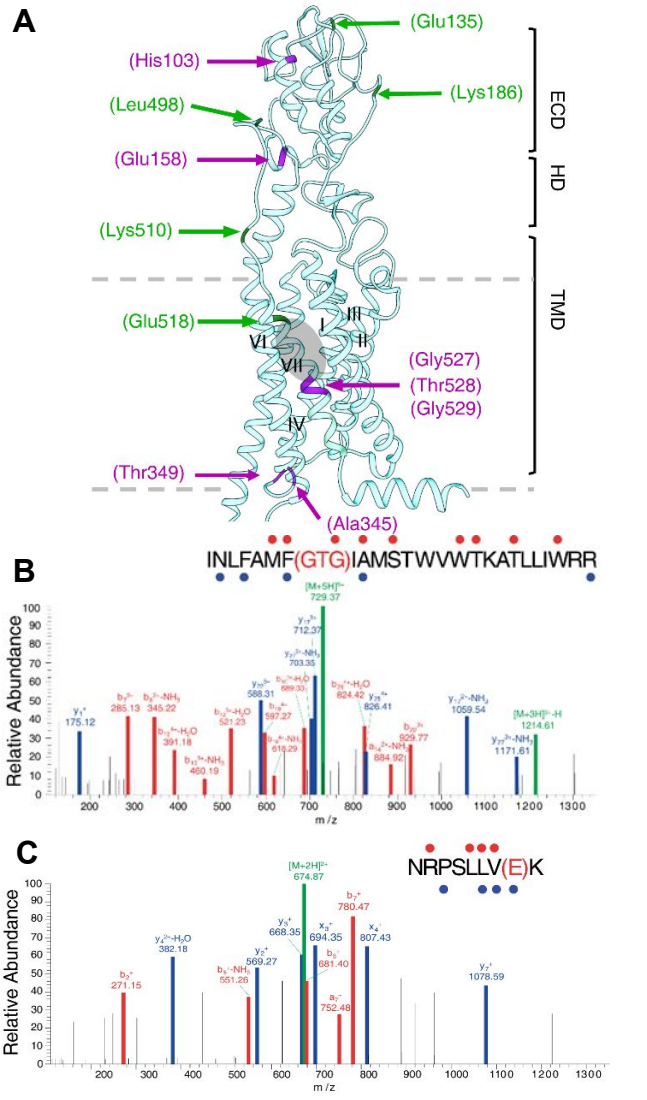

Figure 2. Mass spectrum-based determination of Allo-1 binding site. (A) Multiple residues, labeled with probe **1** (as green) and probe **2** (as violet), were located in distinct regions of SMO (PDB code: 4N4W). The Allo-1 binding site (marked as grey ellipse) located underneath the TMD of SMO was defined by the restriction between E518 and GTG, which were assigned from the MS/MS analysis of probes **1** and probe **2** modified tryptic peptide (C) and (B), respectively.

Allo-1 binds underneath the traditional site of TMD. After radiation with UV light, SMO labeled with probe **1** or **2** was subjected to tryptic digestion. The resulting peptides were analyzed by LC-MS on Thermo Orbitrap Fusion Lumos mass spectrometer. The *m/z* increases of 293.12 and 327.08 were consistent with the molecular weight added by probes **1** and **2**, respectively, after the loss of N_2. We chose the top 10 precursor ions in the MS1 spectra for MS2 acquisition using high-energy collision induced dissociation (HCD) activation. Both probes labeled multiple amino acid residues located in distinct regions of SMO (Table S2, Figure 2A), although many of the labeled residues located in the cytoplasmic domains were likely from non-specific interactions and therefore excluded. Taking advantage of the dual-probe strategy, we identified the true binding site by measuring the distance between the labeled residues by

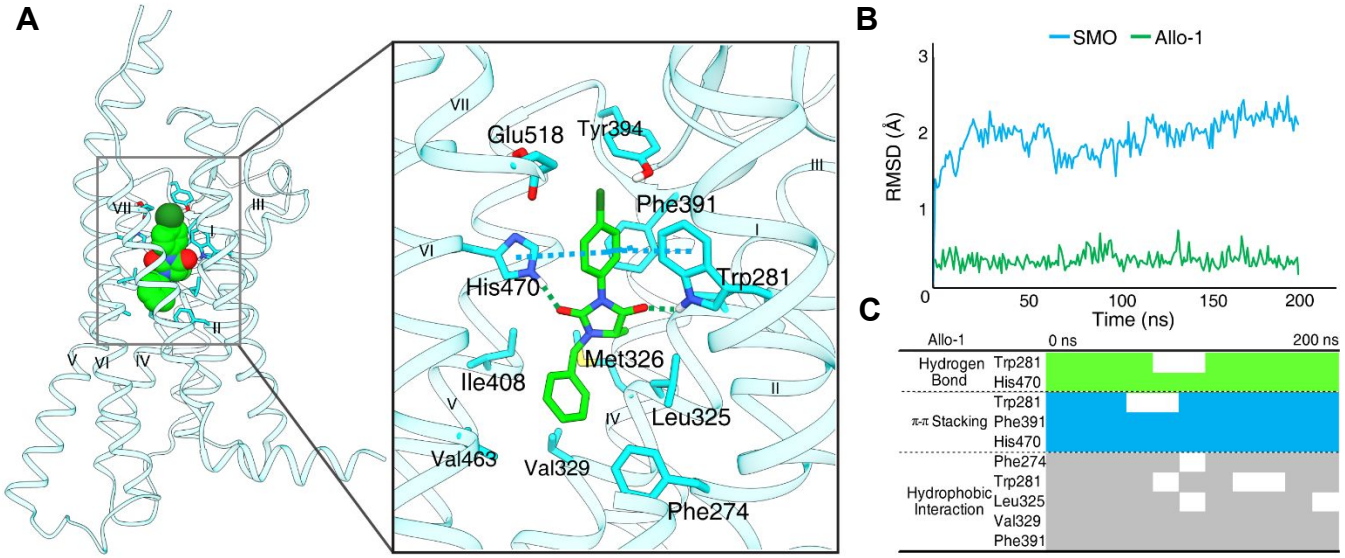

Figure 3. Computational analysis of the underside binding site for Allo-1 (PDB code: 4N4W). (A) Docking of Allo-1 in the defined site of SMO. Close-up view of the Allo-1 (green carbons) binding showed two hydrogen bonds (green dashed lines) and strong π-cage formed with adjacent residues (blue dashed lines). (B) Molecular dynamic simulation showed accurate and stable binding of Allo-1 (green) in SMO (blue). (C) The indicated residues showed continuous corresponding interactions with Allo-1 during 200 ns-simulation.

both probes; as such, the distance should be comparable to the molecular size of Allo-1 (~ 13 Å, Figure S7). After calculating the distance between all the labeled residues from both probes, only two pairs (Glu518 with Gly527 and Thr528 respectively) fell within the range of Allo-1 size (Table S2). Glu518 was assigned from the MS/MS analysis of probe **1** modified peptide ^{511}NRPSLLVEK^{519} Da according to numerous *b*- and *y*-type ions that formed after HCD fragmentation (Figure 2B). Gly527, Thr528, and Gly529 in a slightly longer distance from Glu518, were continuous residues from one same peptide alkylated by probe **2**, indicating a relatively promiscuous pattern and probably freely swinging binding (Figure 2C). Collectively, an underneath binding site was assigned for Allo-1 by the restriction of the upper residue (Glu518) and lower region (Gly527 to Gly529) (Figure 2A).

Key interactions responsible for the binding of Allo-1 within the underside site of SMO. A docking study of Allo-1 was carried out on the defined binding site in SMO (PDB: 4N4W) (Figure 3A). High-density interactions within the compact site were identified, confirming Allo-1 as a potent ligand. In this binding, two pairs of hydrogen bonds were formed between each of carbonyl oxygen with His470 and Trp281. A set of strongly stabilizing π-π interactions were identified between the upper benzene and the adjacent aromatic residues His470, Phe391, and Trp281, which formed a "π-cage". Apart from other ligands, even SANT-1 with a deep binding , Allo-1 did not interact with extracellular loops, and seemed far away from Asp473 (~3.7 Å), whose mutation to histidine will not severely attenuate its binding[23] (Figure S8).

To investigate the binding stability between Allo-1 and SMO, we performed a 200 ns molecular dynamics (MD) simulation (Figure 3B). Allo-1 only showed a 0.3 Å RMSD during the simulation, implying that the binding pose was accurate. Continuous interactions, including hydrogen bond and π-π interaction involving residues His470, Phe391, and Trp281, locked Allo-1 in a stable conformation (Figure 3C). In addition to the π-cage effect, hydrophobic interactions with residues located at the bottom of the pocket, such as Phe274, Leu325, Val329, and Val463, contributed to the tight binding of Allo-1.

Structure-activity relationship (SAR) analysis of Allo-1 analogs within the binding site. To validate the major interactions in the Allo-1 binding, we employed a dissection approach for SAR analysis (Table 1 and Scheme S2)[32]. Allo-1 was dissected into three parts, each of which was chemically mutated so as to weaken the assigned interaction, while maintaining the molecular size.

After replacing the benzene ring with the cyclohexyl group, compounds **5** and **9** showed dramatic loss of activity in the luciferase reporter assay compared with Allo-1. The right benzene seemed even more sensitive to dearomatization, consistent with the loss of the π-π interactions within the π-cage. In parallel, the perfluorated benzene in compounds **6** and **10** led to reduced potency. Perfluorobenzene usually enhances its interaction with benzene via face-to-face packed π-π interaction[33-35]. However, when packed in pure hydrophobic site, such as in the area composed of Val463, Val329, Ile408, Leu325, and Met326, the perfluoroaryl of compound **6** is unfavored due to electrostatic repulsion[36]. The decreased potency of compound **10** indicated the mismatched packing of perfluorobenzene with its interacting aromatic residues. We also attempted the transplacement of the benzenes by tuning the linker to the hydantoin core on the left (**7**-**8**) and right (**11**). The right benzene seemed highly conserved, and a single carbon extension abolished the activity; meanwhile the left benzene was relatively tolerable.

Table 1. SAR analysis of Allo-1 analogs.

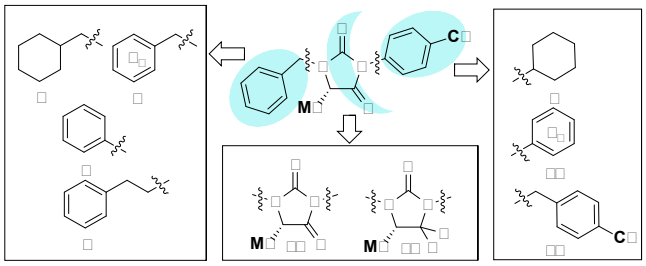

Compds	IC50 (nM)[a]	Compds	IC50 (nM)[a]
Allo-1	59±9	**9**	8006±1994
5	383±109	**10**	1533±262
6	7382±2618	**11**	8097±1921
7	547±453	**12**	3791±673
8	92±38	**13**	4552±2245

[a]The potency of the analogs was evaluated by Gli-luciferase reporter assay. IC_{50} values represent the mean ± SEM of three independent experiments, each conducted in duplicate.

We also investigated the hydrogen bonds between the carbonyls and the protein. When sulfur replaced the urea carbonyl oxygen in compound **12**, the proposed hydrogen bonding with residue His470 was not enforced[37-38]. By contrast, a significant decrease was reflected in the moderate EC_{50}. The gap implied that the tight binding of Allo-1 tolerated no enlarged atom at the carbonyl oxygen[39]. The removal of another carbonyl oxygen in compound **13** also reduced the activity, albeit to a lesser extent, correlating with the disappearance of the corresponding hydrogen bond.

The attenuation of the potency of the Allo-1 analogs was also reflected in the MM-GBSA calculation and docking study (Figure S9, Table S3)[40]. As indicated, the maximum loss of binding free energy, and the lowest docking score clearly reflected the complete disappearance of the π-cage effect in cyclohexyl analog **9** (Figure S9E). The perfluorated benzene replacement (**10**), the transplacement of benzene (**11**), and even the sulfur replacement of urea carbonyl oxygen (**12**), significantly decreased the binding free energy, which originated from the twist of the hydantoin ring or the orientation of the right benzene that disordered the molecular packing.

Allo-1 binding site might be targeted by Allo-2. Similar to Allo-1, Allo-2 (Figure S2) also showed allosteric antagonism activity of SMO[23]. Allo-2 noncompetitively antagonizes SMO induced by SAG while competing with Bodipy-CP (Table S1). Our docking study generated good docking pose with a high score at -11.4 (Figure 4A) in the Allo-1 binding site, similar to Allo-1 score (-11.4, Table S3). In this binding mode, Allo-2 superimposed well with Allo-1. The benzene group and indazole group of Allo-2 occupied the similar places of the two benzene groups of Allo-1, and the pyrimidine group of Allo-2 located in the middle of the pocket similar to hydantoin in Allo-1. A similar π-cage, formed by His470, Phe391, and Trp281, captured the upper benzene group of Allo-2. In addition, two hydrogen bonds were found, namely, between His470 and pyrimidinyl amine in the middle, and between the indazole group of Allo-2 and Thr528 at the bottom of the molecule; these bonds significantly helped stabilize the overall conformation. Though highly overlapped to each other, Allo-2 seems to be longer than Allo-1, with the trifluoromethoxy group on the top, which is probably responsible for competition with CP, making Allo-2 different from Allo-1. The distances between CP and Allo-1 and Allo-2 are 3.8 Å and 1.6 Å, respectively (Figure 4B and 4C). Considering the van der Waals radius of O (1.40 Å) and F (1.35 Å), Allo-2 is sufficiently close to clash with CP and compete for binding, while leaving Allo-1 not interrupted. Additionally, LY0940680 would partially overlap with Allo-1 (Figure S10). Allo-2 showed similar competition binding affinity (K_i= 30±21 nM, Figure S 11) with Allo-1 (K_i= 33±14 nM, Table 1). Meanwhile, Probe **3** specific fluorescent labeling was gradually competed by Allo-2, providing the evidence that Allo-2 targeted in Allo-1 binding site (Figure S12).

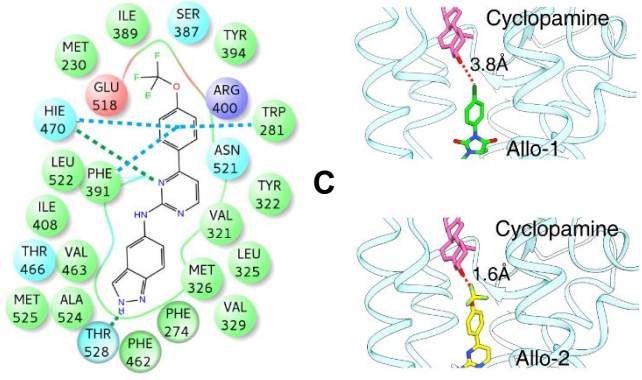

Figure 4. Allo-2 binds to the same site as Allo-1 (PDB code: 4N4W). (A) Close up view of Allo-2 binding showed two hydrogen bonds (green dashes) of pyrimidine and indazole with His470 and Thr528, as well as the π-cage (blue dashes) formed with the upper benzene. The binding of Allo-2 is closer

to CP, as indicated by the distance measured for Allo-1 (B) and Allo-2 (C).

CONCLUSION

Here, we report the identification of an underside pocket of SMO hosting Allo-1 by a cross-disciplinary approach combining mass spectrometry, computational biology and medicinal chemistry. Photoaffinity labeling has been widely used in binding site identification, but is often accompanied by significant non-specific incorporation, as also indicated in each single labeling in this study (Figure 2A). Specific probes are not easily accessed due to the size limitation of the labeling group and sometimes of the ligand itself. Our strategy intrinsically circumvents the misleading, non-specific photolabeling and facilitates docking using a defined orientation of the ligand.

The structural insights of this binding site will open possibilities for development of new design and virtual screening of next-generation anti-cancer drugs against resistant mutants of SMO. Compared with the challenging co-crystallization attempts, we contributed a straightforward and efficient approach to the community of structural biologists. Our methodology should also facilitate the characterization of unknown binding sites of enormous allosteric GPCR modulators that is essential in the understanding of GPCR function and innovative drug discovery.

EXPERIMENTAL SECTION

General. All commercial reagents and solvents were purchased from Accela, J&K, Adamas, Bide and Sigma-Aldrich. Reagents and solvents were used without further purification. High-resolution mass spectra were recorded on an Agilent 6230 mass spectrometer using ESI (electrospray ionization). Chromatography was performed on silica gel 200-300 mesh. NMR spectra were recorded on a Bruker AVANCE III 500, 600 or 800 spectrometer (FT, 500/600/800 MHz for 1H NMR; 126/150/201 MHz for 13C NMR. The purity of all biologically evaluated compounds was determined by HPLC (Shimadzu, LC20AD) and then confirmed with Agilent mass spectrometer (Agilent 6230, TOF, LC/MS). Systems were run with 10%-90% acetonitrile/water gradient with 0.05% TFA. (column: Waters X bridge shield RP 18, 5 μm, column 4.6 × 250 mm; temperature = 25 °C; solvent A = H2O, 0.05% TFA; solvent B = MeCN, 0.05% TFA; flow rate = 1.0 mL/min; method: gradient: 10% B [over 3 min], then 10% B to 90% B [over 2 min], then 90% B [over 10 min]), then 10% B [over 5 min]. For certain substances, optimization of the HPLC gradient was performed. All final compounds showed a purity of >95%. All phenyl isocyanate compounds were obtained from commercial sources or synthesized according to the literature[41].

Please refer to SI for detailed procedures for the synthesis of all intermediates and characterization of all compounds.

General procedure for synthesis of azide compounds (1, 2). To a solution of amino analogs of Allo-1 (**S6** and **S7**) (0.48 mmol) in 0.5 mL 6 N HCl was added dropwise $NaNO_2$ (0.72 mmol, 50 mg) in 3 mL H_2O at 0 °C. Then NaN_3 (0.72 mmol, 47 mg) in 2 mL H_2O was slowly added to the mixture. After that, the reaction was stirred for another 40 minutes at room temperature before being quenched with $NaHCO_3$ solution and extracted with EtOAc three times. The organic layer was washed with brine and dried over Na_2SO_4. Finally, the reaction was concentrated and purified with flash column chromatography (EtOAc/PE 1:3) on silica gel to obtain compounds **1** and **2**.

(S)-3-(4-azidophenyl)-1-benzyl-5-methylimidazolidine-2,4-dione (1) white solid. ^{1}H NMR (500 MHz, Chloroform-*d*), δ (ppm) 7.50-7.43 (m, 2H), 7.42-7.29 (m, 5H), 7.14-7.08 (m, 2H), 5.07 (d, J = 15.2 Hz, 1H), 4.23 (d, J = 15.2 Hz, 1H), 3.95 (q, J = 7.0 Hz, 1H), 1.49 (d, J = 7.0 Hz, 3H); ^{13}C NMR (126 MHz, Chloroform-*d*), δ (ppm) 172.4, 155.1, 139.8, 135.6, 129.2, 128.6, 128.40, 128.36, 127.4, 119.6, 54.7, 44.9, 15.5. HRMS calcd for $C_{17}H_{15}N_5O_2$ $[M+H]^+$: 322.1299; found: 322.1345. HPLC: t_R 11.2 min, purity >95%.

(S)-1-(4-azidobenzyl)-3-(4-chlorophenyl)-5-methylimidazolidine-2,4-dione (2) white solid. ^{1}H NMR (500 MHz, Chloroform-*d*), δ (ppm) 7.45-7.40 (m, 4H), 7.31 (d, J = 8.7 Hz, 2H), 7.03 (d, J = 8.7 Hz, 2H), 4.99 (d, J = 15.3 Hz, 1H), 4.24 (d, J = 15.3 Hz, 1H), 3.96 (q, J = 7.0 Hz, 1H), 1.48 (d, J = 7.0 Hz, 3H); ^{13}C NMR (126 MHz, Chloroform-*d*), δ (ppm) 172.1, 154.9, 140.3, 133.9, 132.3, 130.4, 129.9, 129.3, 127.1, 119.8, 54.8, 44.4, 15.6; HRMS calcd for $C_{17}H_{14}ClN_5O_2$ $[M+H]^+$: 356.0909; found: 356.0906. HPLC: t_R 11.6 min, purity>95%.

Synthesis of Compound 3. To a solution of **S9** (0.068 mmol, 23 mg) in 2 mL acetone was added K_2CO_3 (0.5 M) and 3-bromopropyne (0.14 mmol, 17 mg). The reaction was stirred at room temperature overnight. After that, the reaction was quenched with saturated NH_4Cl solution and extracted with EtOAc three times. The combined organic layer was washed with saturated NH_4Cl solution and brine, dried over Na_2SO_4. Finally, the reaction was concentrated and purified with flash column chromatography (EtOAc/PE 1:3) on silica gel to obtain compound **3**.

(S)-1-(4-azidobenzyl)-5-methyl-3-(4-(prop-2-yn-1-yloxy) phenyl)imidazolidine-2,4-dione (3) yellow solid. ^{1}H NMR (500 MHz, Chloroform-*d*), δ (ppm) 7.36-7.30 (m, 4H), 7.06-7.03 (m, 4H), 4.99 (d, J = 15.3 Hz, 1H), 4.71 (d, J = 2.4 Hz, 2H), 4.24 (d, J = 15.3 Hz, 1H), 3.93 (q, J = 7.0 Hz, 1H), 2.53 (t, J = 2.4 Hz, 1H), 1.47 (d, J = 7.0 Hz, 3H). 13C NMR (126 MHz, Chloroform-d), δ (ppm) 172.5, 157.2, 155.5, 140.3, 132.5, 129.9, 127.5, 125.4, 119.7, 115.5, 78.3, 76.0, 56.2, 54.9, 44.5, 15.6. HRMS calcd for $C_{20}H_{17}N_5O_3$ $[M+H]^+$: 376.1410; found: 376.1409. HPLC: t_R 10.7 min, purity >95%.

ASSOCIATED CONTENT

Supporting Information. This material is available free of charge via the Internet at http://pubs.acs.org.

SMILES strings for the small molecules of Figure 1B and Table 1 (CSV)

AUTHOR INFORMATION

Corresponding Author

*For Y.X., Email, ylxiao@sibs.ac.cn

*For S.Z., Email, zhaosw@shanghaitech.edu.cn
*For H.T., Email, taohch@shanghaitech.edu.cn
ORCID
Houchao Tao: 0000-0001-7598-0275

Author Contributions

†F.Z, K.D. and Y.Z. contributed equally.

Notes

The authors declare no competing financial interest.

ACKNOWLEDGMENT

The authors (FX, SZ and HT) are thankful to Shanghai Municipal Government, ShanghaiTech University for startup financial support, and National Key R&D Program of China (2018YFA0507000) for partial support. This work was also supported by NSFC (21502206, 21572243, YX). We thank J. Liu, Q. Shi, Y. Xu and L. Yang for assistance in the membrane preparation, assay performance, plasmid preparation and NMR data collection respectively at the Core Facility of iHuman Institute. We thank Y. Shan for MS assistance in the core facility center of the Institute of Plant Physiology and Ecology. We thank Y. Zhao for the generous donation of NIH-3T3 cell line for the assay. We thank Z.-J. Liu, G. Song, G. Zhong, D. Wu, D. Liu, J. Cheng and C. Zhang for their insightful discussion and assistance in manuscript preparation.

ABBREVIATIONS

GPCR, G protein-coupled receptor; BODIPY, Difluoro{2-[1-(3,5-dimethyl-2H-pyrrol-2-ylidene-N)ethyl]-3,5-dimethyl-1H-pyrrolato-N}boron.

REFERENCES

1. Briscoe, J.; Therond, P. P., The mechanisms of Hedgehog signaling and its roles in development and disease. *Nat. Rev. Mol. Cell. Biol.* **2013**, *14*, 416-429.
2. Zhao, Y.; Tong, C.; Jiang, J., Hedgehog regulates smoothened activity by inducing a conformational switch. *Nature* **2007**, *450*, 252-258.
3. Ingham, P. W.; McMahon, A. P., Hedgehog signaling in animal development: paradigms and principles. *Genes Dev* **2001**, *15*, 3059-3087.
4. Rubin, L. L.; de Sauvage, F. J., Targeting the hedgehog pathway in cancer. *Nat. Rev. Drug Discovery* **2006**, *5*, 1026-1033.
5. di Magliano, M. P.; Hebrok, M., Hedgehog signaling in cancer formation and maintenance. *Nat. Rev. Cancer* **2003**, *3*, 903-911.
6. Maschinot, C. A.; Pace, J. R.; Hadden, M. K., Synthetic small molecule inhibitors of Hh signaling as anti-cancer chemotherapeutics. *Curr. Med. Chem.* **2015**, *22*, 4033-4057.
7. Robarge, K. D.; Brunton, S. A.; Castanedo, G. M.; Cui, Y.; Dina, M. S.; Goldsmith, R.; Gould, S. E.; Guichert, O.; Gunzner, J. L.; Halladay, J.; Jia, W.; Khojasteh, C.; Koehler, M. F. T.; Kotkow, K.; La, H.; La Londe, R. L.; Lau, K.; Lee, L.; Marshall, D.; Marsters, J. C.; Murray, L. J.; Qian, C.; Rubin, L. L.; Salphati, L.; Stanley, M. S.; Stibbard, J. H. A.; Sutherlin, D. P.; Ubhayaker, S.; Wang, S.; Wong, S.; Xie, M., GDC-0449-A potent inhibitor of the hedgehog pathway. *Bioorg. Med. Chem. Lett.* **2009**, *19*, 5576-5581.
8. Munchhof, M. J.; Li, Q.; Shavnya, A.; Borzillo, G. V.; Boyden, T. L.; Jones, C. S.; LaGreca, S. D.; Martinez-Alsina, L.; Patel, N.; Pelletier, K.; Reiter, L. A.; Robbins, M. D.; Tkalcevic, G. T., Discovery of PF-04449913, a potent and orally bioavailable inhibitor of Smoothened. *ACS Med. Chem. Lett.* **2012**, *3*, 106-111.
9. Pan, S.; Wu, X.; Jiang, J.; Gao, W.; Wan, Y.; Cheng, D.; Han, D.; Liu, J.; Englund, N. P.; Wang, Y.; Peukert, S.; Miller-Moslin, K.; Yuan, J.; Guo, R.; Matsumoto, M.; Vattay, A.; Jiang, Y.; Tsao, J.; Sun, F.; Pferdekamper, A. C.; Dodd, S.; Tuntland, T.; Maniara, W.; Kelleher, J. F., III; Yao, Y.-m.; Warmuth, M.; Williams, J.; Dorsch, M., Discovery of NVP-LDE225, a potent and selective Smoothened antagonist. *ACS Med. Chem. Lett.* **2010**, *1*, 130-134.
10. Sharpe, H. J.; Wang, W.; Hannoush, R. N.; de Sauvage, F. J., Regulation of the oncoprotein Smoothened by small molecules. *Nat. Chem. Biol.* **2015**, *11*, 246-255.
11. Yauch, R. L.; Dijkgraaf, G. J. P.; Alicke, B.; Januario, T.; Ahn, C. P.; Holcomb, T.; Pujara, K.; Stinson, J.; Callahan, C. A.; Tang, T.; Bazan, J. F.; Kan, Z.; Seshagiri, S.; Hann, C. L.; Gould, S. E.; Low, J. A.; Rudin, C. M.; de Sauvage, F. J., Smoothened mutation confers resistance to a Hedgehog pathway inhibitor in medulloblastoma. *Science* **2009**, *326*, 572-574.
12. Dlugosz, A.; Agrawal, S.; Kirkpatrick, P., Vismodegib. *Nat. Rev. Drug Discovery* **2012**, *11*, 437-438.
13. Atwood, S. X.; Sarin, K. Y.; Whitson, R. J.; Li, J. R.; Kim, G.; Rezaee, M.; Ally, M. S.; Kim, J.; Yao, C.; Chang, A. L. S.; Oro, A. E.; Tang, J. Y., Smoothened variants explain the majority of drug resistance in basal cell carcinoma. *Cancer Cell* **2015**, *27*, 342-353.
14. Dijkgraaf, G. J. P.; Alicke, B.; Weinmann, L.; Januario, T.; West, K.; Modrusan, Z.; Burdick, D.; Goldsmith, R.; Robarge, K.; Sutherlin, D.; Scales, S. J.; Gould, S. E.; Yauch, R. L.; de Sauvage, F. J., Small molecule inhibition of GDC-0449 refractory smoothened mutants and downstream mechanisms of drug resistance. *Cancer Res.* **2011**, *71*, 435-444.
15. Byrne, E. F. X.; Luchetti, G.; Rohatgi, R.; Siebold, C., Multiple ligand binding sites regulate the Hedgehog signal transducer Smoothened in vertebrates. *Curr. Opin. Cell Biol.* **2018**, *51*, 81-88.
16. Wang, C.; Wu, H.; Katritch, V.; Han, G. W.; Huang, X.-P.; Liu, W.; Siu, F. Y.; Roth, B. L.; Cherezov, V.; Stevens, R. C., Structure of the human smoothened receptor bound to an antitumor agent. *Nature* **2013**, *497*, 338-343.
17. Wang, C.; Wu, H.; Evron, T.; Vardy, E.; Han, G. W.; Huang, X.-P.; Hufeisen, S. J.; Mangano, T. J.; Urban, D. J.; Katritch, V.; Cherezov, V.; Caron, M. G.; Roth, B. L.; Stevens, R. C., Structural basis for Smoothened receptor modulation and chemoresistance to anticancer drugs. *Nat. Commun.* **2014**, *5*, 4355-4365.
18. Byrne, E. F. X.; Sircar, R.; Miller, P. S.; Hedger, G.; Luchetti, G.; Nachtergaele, S.; Tully, M. D.; Mydock-McGrane, L.; Covey, D. F.; Rambo, R. P.; Sansom, M. S. P.; Newstead, S.; Rohatgi, R.; Siebold, C., Structural basis of Smoothened regulation by its extracellular domains. *Nature* **2016**, *535*, 517-522.
19. Huang, P.; Nedelcu, D.; Watanabe, M.; Jao, C.; Kim, Y.; Liu, J.; Salic, A., Cellular cholesterol directly activates Smoothened in Hedgehog signaling. *Cell* **2016**, *166*, 1176-1187.
20. Zhang, X.; Zhao, F.; Wu, Y.; Yang, J.; Han, G. W.; Zhao, S.; Ishchenko, A.; Ye, L.; Lin, X.; Ding, K.; Dharmarajan, V.; Griffin, P. R.; Gati, C.; Nelson, G.; Hunter, M. S.; Hanson, M. A.; Cherezov, V.; Stevens, R. C.; Tan, W.; Tao, H.; Xu, F., Crystal structure of a multi-domain human smoothened receptor in complex with a super stabilizing ligand. *Nat. Commun.* **2017**, *8*, 15383-15392.
21. Huang, P.; Zheng, S.; Wierbowski, B. M.; Kim, Y.; Nedelcu, D.; Aravena, L.; Liu, J.; Kruse, A. C.; Salic, A., Structural basis of Smoothened activation in Hedgehog signaling. *Cell* **2018**, *174*, 312–324.
22. Dong, X.; Wang, C.; Chen, Z.; Zhao, W., Overcoming the resistance mechanisms of Smoothened inhibitors. *Drug Disc. Today* **2018**, *23*, 704-710.
23. Tao, H.; Jin, Q.; Koo, D.-I.; Liao, X.; Englund, N. P.; Wang, Y.; Ramamurthy, A.; Schultz, P. G.; Dorsch, M.; Kelleher, J.; Wu, X., Small molecule antagonists in distinct binding modes

inhibit drug-resistant mutant of Smoothened. *Chem. Biol.* **2011**, *18*, 432-437.

24. Chen, J. K.; Taipale, J.; Young, K. E.; Maiti, T.; Beachy, P. A., Small molecule modulation of Smoothened activity. *Proc. Natl. Acad. Sci.* **2002**, *99*, 14071-14076.

25. Chen, J. K.; Taipale, J.; Cooper, M. K.; Beachy, P. A., Inhibition of hedgehog signaling by direct binding of cyclopamine to smoothened. *Genes Dev.* **2002**, *16*, 2743-2748.

26. Leitner, A., Cross-linking and other structural proteomics techniques: how chemistry is enabling mass spectrometry applications in structural biology. *Chem. Sci.* **2016**, *7*, 4792-4803.

27. Couvineau, A.; Tan, Y.-V.; Ceraudo, E.; Laburthe, M., Strategies for studying the ligand binding site of GPCRs: photoaffinity labeling of the VPAC1 receptor, a prototype of class B GPCRs. *Methods Enzymol.* **2013**, *520* (G Protein Coupled Receptors), 219-239.

28. Gilchrist, T. L.; Rees, C. W., *Carbenes, Nitrenes, and Arynes (Studies in Modern Chemistry)*. Nelson (London): **1969**, pp 131.

29. Bayley, H.; Knowles, J. R., Photogenerated reagents for membrane labeling. 2. Phenylcarbene and adamantylidene formed within the lipid bilayer. *Biochemistry* **1978**, *17*, 2420-2423.

30. Dong, M.; Miller, L. J., Use of photoaffinity labeling to understand the molecular basis of ligand binding to the secretin receptor. *Ann. N. Y. Acad. Sci.* **2006**, *1070* (VIP, PACAP, and Related Peptides), 248-264.

31. Grunbeck, A.; Sakmar, T. P., Probing G protein-coupled receptor-ligand interactions with targeted photoactivatable cross-linkers. *Biochemistry* **2013**, 52, 8625-8632.

32. Ye, L.; Ding, K.; Zhao, F.; Liu, X.; Wu, Y.; Liu, Y.; Xue, D.; Zhou, F.; Zhang, X.; Stevens, R. C.; Xu, F.; Zhao, S.; Tao, H., A structurally guided dissection-then-evolution strategy for ligand optimization of smoothened receptor. *MedChemComm* **2017**, *8*, 1332-1336.

33. Coates, G. W.; Dunn, A. R.; Henling, L. M.; Dougherty, D. A.; Grubbs, R. H., Phenyl-perfluorophenyl stacking interactions: a new strategy for supermolecule construction. *Angew. Chem., Int. Ed.* **1997**, *36*, 248-251.

34. Pace, C. J.; Gao, J., Exploring and exploiting polar-π interactions with fluorinated aromatic amino acids. *Acc. Chem. Res.* **2013**, *46*, 907-915.

35. Zheng, H.; Comeforo, K.; Gao, J., Expanding the fluorous arsenal: tetrafluorinated phenylalanines for protein design. *J. Am. Chem. Soc.* **2009**, *131*, 18-19.

36. Kim, C.-Y.; Chang, J. S.; Doyon, J. B.; Baird, T. T., Jr.; Fierke, C. A.; Jain, A.; Christianson, D. W., Contribution of fluorine to protein-ligand affinity in the binding of fluoroaromatic inhibitors to carbonic anhydrase II. *J. Am. Chem. Soc.* **2000**, *122*, 12125-12134.

37. Xie, J.; Okano, A.; Pierce, J. G.; James, R. C.; Stamm, S.; Crane, C. M.; Boger, D. L., Total synthesis of [ψ[C(=S)NH]Tpg4]Vancomycin Aglycon, [ψ[C(=NH)NH]Tpg4]Vancomycin Aglycon, and related key compounds: reengineering vancomycin for dual D-Ala-D-Ala and D-Ala-D-Lac binding. *J. Am. Chem. Soc.* **2012**, *134*, 1284-1297.

38. Xie, J.; Pierce, J. G.; James, R. C.; Okano, A.; Boger, D. L., A redesigned vancomycin engineered for dual D-Ala-D-Ala and D-Ala-D-Lac binding exhibits potent antimicrobial activity against vancomycin-resistant bacteria. *J. Am. Chem. Soc.* **2011**, *133*, 13946-13949.

39. Lee, H.-J.; Choi, Y.-S.; Lee, K.-B.; Park, J.; Yoon, C.-J., Hydrogen bonding abilities of thioamide. *J. Phys. Chem. A* **2002**, *106*, 7010-7017.

40. Huang, N.; Kalyanaraman, C.; Bernacki, K.; Jacobson, M. P., Molecular mechanics methods for predicting protein-ligand binding. *Phys. Chem. Chem. Phys.* **2006**, 8, 5166-5177.

41. Liu, D. Z.; Tian, Z.; Yan, Z. H.; Wu, L. X.; Ma, Y.; Wang, Q.; Liu, W.; Zhou, H. G.; Yang, C., Design, synthesis and evaluation of 1,2-benzisothiazol-3-one derivatives as potent caspase-3 inhibitors. *Bioorg. Med. Chem.* **2013,** *21*, 2960-2967.